# UC Berkeley
## UC Berkeley Previously Published Works

**Title**

Comparing Experimental Phase Behavior of Ion-Doped Block Copolymers with Theoretical Predictions Based on Selective Ion Solvation

**Permalink**

https://escholarship.org/uc/item/81f3824s

**Journal**

Macromolecules, 53(10)

**ISSN**

0024-9297

**Authors**

Hou, Kevin J
Loo, Whitney S
Balsara, Nitash P
et al.

**Publication Date**

2020-05-26

**DOI**

10.1021/acs.macromol.0c00559

Peer reviewed

# Comparing experimental phase behavior of ion-doped block copolymers with theoretical predictions based on selective ion solvation

Kevin J. Hou,*,† Whitney S. Loo,‡ Nitash P. Balsara,‡ and Jian Qin*,†

†*Department of Chemical Engineering, Stanford University, Stanford, CA 94305*

‡*Department of Chemical and Biomolecular Engineering, University of California – Berkeley, Berkeley, CA 94720*

E-mail: kjhou@stanford.edu; jianq@stanford.edu

## Abstract

The effects of salt-doping on the morphological behavior of block copolymers are well established but remain poorly understood, partially due to the challenge of resolving electrostatics in a heterogeneous medium with low average permittivity. Employing recently-developed field theory, we analyze the phase behavior of polystyrene-*b*-poly(ethylene oxide) (SEO) copolymers doped with lithium bis(trifluoromethane sulfonyl)imide salts (LiTFSI). Using a single fitting parameter, the ionic solvation radius, we obtain qualitative agreement between our theory and experimental data over a range of polymer molecular weights and copolymer compositions. Such agreement supports and highlights the need of solvation free energy to accurately describe the self-assembly of ion-doped block copolymers, and demonstrates that experimentally observed dependence on molecular weight, not present in neutral block copolymers, can be rationalized by solvation effects. Overall morphological variations are stronger

than those predicted by the leading, linear order theory, but can be captured by the full model.

# Introduction

Although the phase behavior of neutral block copolymers and those diluted with neutral solvents are well characterized,[1–4] our understanding of salt-doped block copolymers remains incomplete. Experimental observations of salt-doped copolymers reveal a variety of morphological behaviors, including enhanced incompatibility between unlike blocks,[5] drastically increased domain spacing,[6] and ion-induced morphological variation.[7,8] Though substantial theoretical efforts have been made to explain this phenomenology, no single theory has been able to capture all of these experimental findings. However, owing to the series of works by Wang et al.,[9–12] it is clear that the solvation free energy of ions plays a prominent role in dictating the thermodynamics of salt-doped polymers. Explicitly accounting for the solvation free energy increases the incompatibility between the composing polymer blocks. To leading order, this effect has been accounted for by introducing an effective Flory-Huggins $\chi$ parameter $\chi_{\text{eff}}$ that increases linearly with salt concentration. This linear scaling is commonly employed to rationalize experimental results.[8,13,14]

In prior works, the linear scaling of $\chi_{\text{eff}}$ has successfully captured trends in experimentally determined domain spacing,[10] as well as salt-induced changes in morphology.[14] However, estimates of $\chi_{\text{eff}}$ from scattering[13] suggest that the dependence of $\chi_{\text{eff}}$ on salt concentration is highly nonlinear, especially at elevated salt concentrations. Similarly, more recent theories[15–17] have shown that salt-induced, nonlinear shifts in block copolymer phase behavior cannot be rationalized using a single effective $\chi$ parameter. It becomes imperative to resolve these discrepancies using experimental data.

A comprehensive description of salt-containing block copolymers is challenging because these materials exhibit strong, heterogeneous electrostatic interactions. Ordered mesophases

of these block copolymers are typically characterized by dielectric inhomogeneity on length-scales of 10–50 nanometers and, in general, dielectric screening of electrostatic interactions is weak because the permittivity of polymers is low. To address this multitude of challenges, a number of theoretical efforts have been made, each with varying approaches to model such strong, heterogeneous electrostatics. These theories are summarized in the following.

The first theoretical approach that attempted to capture the aforementioned experimental trends incorporates charge dissociation, ion binding, and ion solvation into the canonical self-consistent field theory (SCFT) for neutral block copolymers.[9–12] Ions were treated as reversibly bound to polymer chains, and electrostatics were treated at the Poisson-Boltzmann level. For near-symmetric ($f = 0.5$) ion-containing diblock copolymers, this theory incorporates the effects of salt-doping into an effective $\chi$ parameter, which successfully captures experimentally observed increases in domain spacing and order-disorder transition temperature due to increases in salt concentration.

This field theory neglects the strong ionic correlations that are important in low permittivity materials. At low salt concentrations, such correlations are captured by the Debye-Hückel theory.[18] As a reference, in polystyrene-$b$-poly(ethylene oxide) mixed with lithium bis(trifluoromethanesulfonyl)imide salt, hereafter referred to as SEO/LiTFSI, a simple scaling argument[17] shows that the Debye-Hückel correlation breaks down at most experimentally relevant ion concentrations, e.g. molar ratios of $r \equiv [\mathrm{Li}]/[\mathrm{EO}] \sim 0.10$–$0.20$. Thus, a correction for correlation effects is needed. In an alternative approach, a liquid-state theory based correction for ionic correlations has been incorporated into a block copolyelectrolyte model, leading to a hybrid 'liquid state + SCFT' theory.[16,19–22] This model predicts a stable 'chimney-like' regime for diblock polyelectrolytes: a narrow channel of ordered phases is predicted to be stable for diblocks with a majority low-dielectric block, even when the two blocks are compatible or nearly so. This behavior was attributed to 'electrostatic cohesion', the hypothesis that ionic clusters, which enter the model through liquid-state correlations, stabilize ordered phases of the block polyelectrolyte.

In a third approach, liquid-state theory was combined with classical fluids density functional theory (fDFT) to describe ion-containing block copolymers.[23] A coarse-grained $1/r^4$ potential was introduced to describe ionic solvation, and the results of MD simulations were compared to the predictions of fDFT. Using this framework, the stabilization of the lamellar phase and the increase in domain spacing with salt concentration predicted by the linear theory are confirmed. In the high salt concentration regime, however, lamellar domain spacing saturates.

Recently, the wealth of experimental data on the morphological behavior of ion-doped copolymers[24–27] has been compiled,[14] but not yet analyzed within the framework of the aforementioned theories. Table 1 lists the relevant copolymer properties for the compiled dataset. Careful comparison between this compiled experimental data and each theoretical framework is crucial for evaluating the relative importance of the varied physics which contribute to the thermodynamic phase behavior of ion-doped polymers.

We have recently developed a field theory for ion-doped polymers which relaxes the bound-ion assumption, and illuminates the competition between the ionic solvation and the translational entropy of ions.[17] The work clearly identifies most experimentally relevant systems, such as SEO/LiTFSI, as being dominated by ionic solvation, and predicts nonlinear shifts in phase behavior which can be attributed to ionic solvation alone. Using this framework, complete phase diagrams have been produced for a range of salt concentrations and dielectric contrasts, showing that salt-induced morphological variation in block copolymers is highly nonlinear.

In this work, we present an analysis of the compiled experimental morphology data (Table 1) for ion-doped block copolymers using our 'free ion' model.[17] This theory adopts the minimal model required to treat crucial physics in ion-containing block copolymers. While important ionic solvation effects are considered at the level of the Born solvation model, our theory neglects known complicating effects such as complexation of lithium ions with EO groups,[30–34] the formation of negative clusters and ion-pairs,[35–38] complex solvation effects

4

Table 1: Molecular parameters of experimental systems used in this study.

| $M_{\mathrm{PEO}}$ (kg/mol) | $M_{\mathrm{PS}}$ (kg/mol) | $N$ | $f_{\mathrm{EO}}$ | Reference |
|---|---|---|---|---|
| 0.8 | 1.9 | 42 | 0.29 | Teran[13] |
| 1.6 | 1.4 | 46 | 0.52 | Teran[13] |
| 1.4 | 1.7 | 48 | 0.44 | Teran[13] |
| 3.3 | 2.9 | 94 | 0.52 | Teran[13] |
| 5.5 | 4.9 | 158 | 0.52 | Teran[13] |
| 8.2 | 3.8 | 181 | 0.68 | Loo[28] |
| 2.4 | 9.4 | 184 | 0.20 | Loo[8,28] |
| 4.0 | 9.4 | 208 | 0.29 | Loo[8,28] |
| 4.5 | 10.0 | 224 | 0.30 | Young[29] |
| 12.8 | 5.1 | 269 | 0.72 | Loo[28] |

due to polymer chain connectivity,[39,40] and strong ion-ion correlations.[16,19–22] In addition, the simplest linear mixing rule for dielectric permittivity is employed. With these limitations in mind, the comparison between theory and experiment is expected to establish a baseline for the effects of ionic solvation on the phase behavior of ion-doped block copolymers. By employing the simple Born solvation model, we are able to broadly capture solvation effects with a single adjustable parameter. Our analysis demonstrates that ion solvation captures the majority of experimentally observed morphological variation, and highlights strong non-linear effects that cannot be captured by a single effective $\chi$ parameter. The rest of this paper is organized as follows. The next two sections introduce our model formalism using a presentation based on density functionals, and summarize its main predictions. The following three sections are devoted to the comparison between our model predictions and experimental results, and focus on parameter matching, the effects of salt concentration, and the effects of molecular weight, respectively. The final section summarizes the main findings of this work, highlights limitations of our approach, and proposes future steps to address these limitations.

# The 'free ion' model

Our analyses of experimental data are based on our recently developed 'free ion' model.[17] For brevity, we highlight only important features of this model, deferring a full description of the theory to ref. 17. The model treats ion-doped copolymers as a heterogeneous dielectric medium containing fully mobile ions. This theory extends the canonical SCFT for neutral block copolymers to mixtures of block copolymers and salts. The model Hamiltonian is a sum of four terms, $\mathcal{H} = \mathcal{H}_0 + U_{\mathrm{FH}} + U_{\mathrm{B}} + U_{\mathrm{C}}$, where $\mathcal{H}_0$ is the ideal chain stretching energy, $U_{\mathrm{FH}}$ the Flory-Huggins interaction energy, $U_{\mathrm{B}}$ the ion solvation free energy, and $U_{\mathrm{C}}$ the Coulomb potential energy. We treat ions as small charged particles with a finite volume. The primary difference between this model and previous treatments[9–12,16,19–22] is that ions are not explicitly bound to polymer chains ('free ions'), and that complexation between lithium ions and PEO-like motifs is fully incorporated into the solvation free energy. This results in a simpler treatment of the interaction between cations and polymers that fully retains the translational entropy of ions. The solvation free energy provides a thermodynamic driving force for ions to localize within regions of high dielectric permittivity. For simplicity, we use the Born solvation model,[41] which scales inversely with local medium permittivity and the ion solvation radius. This is conceptually similar to treating ions as a selective solvent, with the crucial distinction that the solvation energy is nonlinearly coupled to polymer concentration through the inverse dielectirc permittivity, $1/\varepsilon_{\mathrm{r}}$. Although previous works have treated the solvation radius as the size of ions estimated from crystallographic data,[12] we instead view it as an emergent mesoscopic parameter determined by fitting against experiments.

Following the standard procedure, the Hamiltonian above can be shown to produce a mean-field free energy density of the form[17]

$$F[\phi(\boldsymbol{r})] = F_0[\phi(\boldsymbol{r})] + F_{\mathrm{int}}[\phi(\boldsymbol{r})]. \tag{1}$$

For salt-doped diblock copolymers in particular, the monomer density field vector $\phi(\boldsymbol{r})$ has

four components $(\phi_+, \phi_-, \phi_A, \phi_B)$ representing the densities of cations, anions, PEO-like, and PS-like polymer blocks. The term $F_0$ is the free energy density of a mixture of non-interacting cations, anions, and copolymers. In terms of polymeric and ionic densities, the non-interacting free energy density per reference volume $v$ can be written

$$F_0 = \frac{\bar{\phi}_{\mathrm{p}}}{N} F_{\mathrm{chain}}[\phi_A(\boldsymbol{r}), \phi_B(\boldsymbol{r})] + \frac{1}{V} \int \mathrm{d}\boldsymbol{r} \left[ \frac{\phi_+(\boldsymbol{r})}{\tilde{v}_+} \ln \phi_+(\boldsymbol{r}) + \frac{\phi_-(\boldsymbol{r})}{\tilde{v}_-} \ln \phi_-(\boldsymbol{r}) \right]. \tag{2}$$

The first term on the right is the contribution to free energy from polymer configurational entropy: $\bar{\phi}_{\mathrm{p}}$ is the overall volume fraction of polymer, $N \equiv V_{\mathrm{p}}/v$ is the number of repeat units of reference volume $v$, where $V_{\mathrm{p}}$ is the polymer volume, and $F_{\mathrm{chain}}$ depends on the partition function of a single polymer chain, which is itself solely determined by the spatially varying density fields of the two polymer blocks, $\phi_A(\boldsymbol{r})$ and $\phi_B(\boldsymbol{r})$. The remaining terms represent the translational entropy of cations and anions: $\tilde{v}_+ \equiv V_+/v$ and $\tilde{v}_- \equiv V_-/v$ are the ionic volumes, and $\phi_+(\boldsymbol{r})$ and $\phi_-(\boldsymbol{r})$ are the density fields of cations and anions, respectively. Note that the free energy expressions above, and in all of the following, have energy units of $k_{\mathrm{B}}T$.

At the mean field level, the free energy due to interactions has an identical functional form to the interacting component of the Hamiltonian, and consists of three terms:

$$F_{\mathrm{int}} = F_{\mathrm{FH}} + F_{\mathrm{B}} + F_{\mathrm{C}}. \tag{3}$$

The Flory-Huggins free energy adopts its standard form, $F_{\mathrm{FH}} = \rho\chi \int \mathrm{d}\boldsymbol{r}\phi_A(\boldsymbol{r})\phi_B(\boldsymbol{r})$, where $\chi$ is the Flory-Huggins parameter between A and B blocks, and $\rho \equiv 1/V$ is a normalizing density. Under this convention, both the free energy and $\chi$ parameter are specified on a per-reference volume basis, i.e. doubling $v$ would also double $\chi$. We do not impose the Flory-Huggins interaction between ions and polymers, with the understanding that such local ion-polymer interactions are absorbed into the ion solvation free energy. Likewise, no Flory-Huggins interaction is imposed between cations and anions, since those pairwise terms

are dominated by the Coulombic interaction.

The solvation free energy per reference volume is given, under the Born approximation, by

$$F_{\mathrm{B}} = \frac{\rho l_0}{2} \int \mathrm{d}\boldsymbol{r} \left[ \frac{\phi_+(\boldsymbol{r})}{\varepsilon_{\mathrm{r}}(\boldsymbol{r})\tilde{v}_+ a_+} + \frac{\phi_-(\boldsymbol{r})}{\varepsilon_{\mathrm{r}}(\boldsymbol{r})\tilde{v}_- a_-} \right]. \tag{4}$$

Here $l_0 \equiv e^2/(4\pi\epsilon_0 k_{\mathrm{B}}T)$ is the vacuum Bjerrum length, and $a_+$ and $a_-$ are the solvation radii of cation and anion respectively. Note that $n_+(\boldsymbol{r}) \equiv (\phi_+(\boldsymbol{r})/\tilde{v}_+)$ and $n_-(\boldsymbol{r}) \equiv (\phi_-(\boldsymbol{r})/\tilde{v}_-)$ are the corresponding number densities of cations and anions, with units of number per reference volume, $v$. The local relative dielectric permittivity is, for simplicity, treated as a density weighted average

$$\varepsilon_{\mathrm{r}}(\boldsymbol{r}) = \frac{\varepsilon_{\mathrm{A}}\phi_{\mathrm{A}}(\boldsymbol{r}) + \varepsilon_{\mathrm{B}}\phi_{\mathrm{B}}(\boldsymbol{r})}{\phi_{\mathrm{A}}(\boldsymbol{r}) + \phi_{\mathrm{B}}(\boldsymbol{r})} \tag{5}$$

Although more elaborate mixing rules are sometimes employed, such as the Clausius-Mossotti relation[9,42,43] or the Landau 1/3-power mixing rule,[44,45] no significant differences are anticipated relative to linear mixing. It should be cautioned that the Born solvation model, as well as this dielectric mixing rule, are continuum models which may not be accurate for heterogeneity at the molecular scale. We revisit this point in our discussion of ionic structure in the conclusion. The important point here is that coupling permittivity to polymer density profiles explicitly introduces dielectric heterogeneity. The bulk permittivities $\varepsilon_{\mathrm{A}}$ and $\varepsilon_{\mathrm{B}}$ are reported in experimental literature, but the solvation radii are treated as adjustable in our model. A more detailed discussion on this point follows below, alongside our analyses of experimental data.

The Coulombic interaction is given by

$$F_{\mathrm{C}} = \frac{\rho}{2} \int \mathrm{d}\boldsymbol{r} \, \rho_q(\boldsymbol{r})\psi(\boldsymbol{r}), \tag{6}$$

where $\rho_q(\boldsymbol{r}) \equiv z_+\phi_+(\boldsymbol{r})/\tilde{v}_+ + z_-\phi_-(\boldsymbol{r})/\tilde{v}_-$ is the charge density with $\tilde{v}_+$ and $\tilde{v}_-$ being the relative volumes of cations and anions with respect to the reference volume $v$, $z_+$ and $z_-$ are the valencies of ions, and $\psi(\boldsymbol{r})$ is the static electric potential. The potential is obtained from

solution of Poisson's equation with heterogeneous dielectric permittivity, i.e.,

$$-\frac{v}{4\pi l_0}\nabla \cdot \varepsilon_{\mathrm{r}}(\boldsymbol{r})\nabla\psi(\boldsymbol{r}) = \rho_{\mathrm{q}}(\boldsymbol{r}) \ . \tag{7}$$

Above, $\psi(\boldsymbol{r})$ is the electrostatic potential energy field, $\rho_{\mathrm{q}}(\boldsymbol{r})$ is the charge density, and $\varepsilon_{\mathrm{r}}(\boldsymbol{r})$ is the spatially varying dielectric permittivity. The prefactor $v/(4\pi l_0)$ fixes $\psi(\boldsymbol{r})$ to be dimensionless. In general, $\varepsilon_{\mathrm{r}}(\boldsymbol{r})$ is coupled to polymer morphology, which is represented by the polymer density fields $\phi_{\mathrm{A}}(\boldsymbol{r})$ and $\phi_{\mathrm{B}}(\boldsymbol{r})$. Since the density fields $\boldsymbol{\phi}(\boldsymbol{r})$ are generated self-consistently from these interaction terms, Eq. (7) is essentially a Poisson-Boltzmann equation for the Coulombic interaction.

Using the free energy defined in Eqs. (1–7), SCFT prescribes a system of equations which can be iteratively solved to obtain candidate equilibrium morphologies of ion-doped diblock copolymers. In particular, solving Eq. (7) at each SCFT iteration is computationally burdensome, especially for three-dimensional morphologies. To address this issue, we have developed a symmetry-adapted algorithm[17,46] to efficiently compute the electric potential. Without loss of generality, Eq. (7) can be expanded in discrete Fourier space as

$$\rho_{\mathrm{q}}(\boldsymbol{r}) = \sum_{\alpha}\rho_\alpha e^{i\boldsymbol{q}_\alpha\cdot\boldsymbol{r}} = \sum_{\alpha}\sum_{\beta}(\boldsymbol{q}_\alpha\cdot\boldsymbol{q}_\beta)\varepsilon_{\alpha-\beta}\psi_\beta e^{i\boldsymbol{q}_\alpha\cdot\boldsymbol{r}} \ . \tag{8}$$

In the above, the subscripts $\alpha$ and $\beta$ denote coefficients corresponding to the wavevectors $\boldsymbol{q}_\alpha$ and $\boldsymbol{q}_\beta$. Eq. (8) can be equivalently rewritten as the matrix multiplication $\rho_\alpha = \mathbf{A}_{\alpha\beta}\psi_\beta$ where $\mathbf{A}_{\alpha\beta} \equiv (\boldsymbol{q}_\alpha\cdot\boldsymbol{q}_\beta)\varepsilon_{\alpha-\beta}$, and $\rho_\alpha$ is the $\alpha$-indexed vector of Fourier coefficients for the charge density. Computing the potential $\psi(\boldsymbol{r})$ reduces to inversion of the $n\times n$ matrix $\mathbf{A}$, where $n$ is the user-selected discretization imposed in numerical calculation. Using the matrix-based representation is advantageous because the underlying symmetry of block copolymer morphology can be readily exploited. We observe that both the dielectric permittivity $\varepsilon_\alpha$ and the charge density $\rho_\alpha$ must respect the symmetry of the unit cell.[46,47] This imposes constraints on the coefficient vectors $\rho_\alpha$ and $\varepsilon_\alpha$. For example, the lamellar morphology requires

9

inversion symmetry, i.e., $\varepsilon_r(\boldsymbol{q}_\alpha) = \varepsilon_r(\boldsymbol{q}_\beta)$. Similar, but more complex relationships can be derived for more complicated morphologies based on their space group symmetry. These symmetry relationships can be used to reduce the dimensionality of $\mathbf{A}$, which substantially improves both efficiency and stability of the numerical solution for Eq. (7).

## Entropic and solvation regimes

Evaluating Eqs. (1–3) for different density fields $\boldsymbol{\phi}(\boldsymbol{r})$ gives the free energy of different morphologies. The only term ~~depending~~ which directly depends on polymer molecular weight is the ideal chain contribution to free energy, which scales with $1/N$. The interacting terms scale with the interaction parameters $\chi$ and $l_0$, and the solvation radii $a_+$ and $a_-$, but not directly with $N$. The ion-ion Coulomb term in Eq. (3) has indirect $N$ dependence because the gradients in Poisson's equation, Eq. (7), scale with $R_g$, the polymer radius of gyration. This is why, for neat block copolymers, the mean field free energy depends on the product $\chi N$. In our 'free-ion' model for salt-doped copolymers, ions are treated with explicit volume, leading to a multi-component system without direct analogy to neat block copolymers. However, note that by setting $l_0$ to vanish (i.e. turning 'off' electrostatic interactions), our model reduces to the SCFT for a block copolymer diluted by a non-selective neutral solvent, as considered by Fredrickson and Leibler.[48] For this system it was shown, by expanding the free energy near the critical point with respect to density fluctuations, that (1) solvents are localized near the interface between incompatible polymer blocks, (2) the amplitude of the solvent density wave is smaller than that of the polymer by a factor of $1/N$, and (3) the variation in phase behavior due to neutral solvent addition can be fully accounted for by rescaling $\chi N$ with the solvent volume fraction (dilution approximation[48]). In the following, we discuss how turning on electrostatic interactions complicates this picture and alters the morphological behavior of salt-doped block copolymers.

Anticipating the importance of the solvation free energy, we introduce a parameter $\lambda_B$ to

quantify the relative solvation free energy for both anions and cations, which is defined as[17]

$$\lambda_\mathrm{B} \equiv \frac{l_0}{2} \left( \frac{\varepsilon_\mathrm{A} - \varepsilon_\mathrm{B}}{\varepsilon_\mathrm{A} \varepsilon_\mathrm{B}} \right) \left( \frac{1}{a_+} + \frac{1}{a_-} \right) . \tag{9}$$

Here, the prefactor $l_0$ is the vacuum Bjerrum length defined in the previous section. The second term reflects the dielectric contrast between polymer components, and is equivalent to $1/\varepsilon_\mathrm{B} - 1/\varepsilon_\mathrm{A}$. The third term represents the average strength of the Born solvation free energy for cations and anions, parameterized by the solvation radii $a_+$ and $a_-$. The parameter $\lambda_\mathrm{B}$ controls the strength of the solvation free energy $F_\mathrm{B}$. The Coulombic interaction between solvated ions $F_\mathrm{C}$, also depends on $l_0$, but this contribution is not as important, because cationic and anionic charges tend to neutralize each other locally (see Fig. 2 below).

Our calculations[17] reveal competition between two distinct thermodynamic regimes, depending primarily on the magnitude of $\lambda_\mathrm{B}$. The key results are reproduced in Fig. 1. These phase diagrams show the disordered phase (DIS), as well as ordered lamellar (L), cylindrical (C), gyroidal (G), and BCC spherical (S) phases. In the 'entropic regime', at $\lambda_\mathrm{B} = 1.9$, the boundary of the ordered phases are shifted towards the 'upper-right' corner, i.e., towards higher $\chi N$ and majority high-permittivity compositions. In the 'solvation regime', at $\lambda_\mathrm{B} = 5.6$, the boundary is shifted towards the 'lower-left', demonstrating the opposite trend. The transition between the two regimes occurs within the range $3 < \lambda_\mathrm{B} < 4$. The origin of such contrasting behavior is the relative free energy difference of selectively solvating ions in the high-permittivity medium.[17] In the 'entropic' regime, where $\lambda_\mathrm{B} < 3$, ion translational entropy dominates and the addition of ions destabilizes ordered phases. In the 'solvation' regime, where $\lambda_\mathrm{B} > 4$, ion solvation energy dominates, and adding ions drives the system to form ordered phases. Notably, our model predicts stabilization of ordered phases at high salt concentrations even as $\chi N \to 0$. These regimes are clearly visible in Fig. 1, where phase diagrams representative of each regime are compared.

In both regimes, the variation in phase behavior upon the addition of salt is asymmetric,
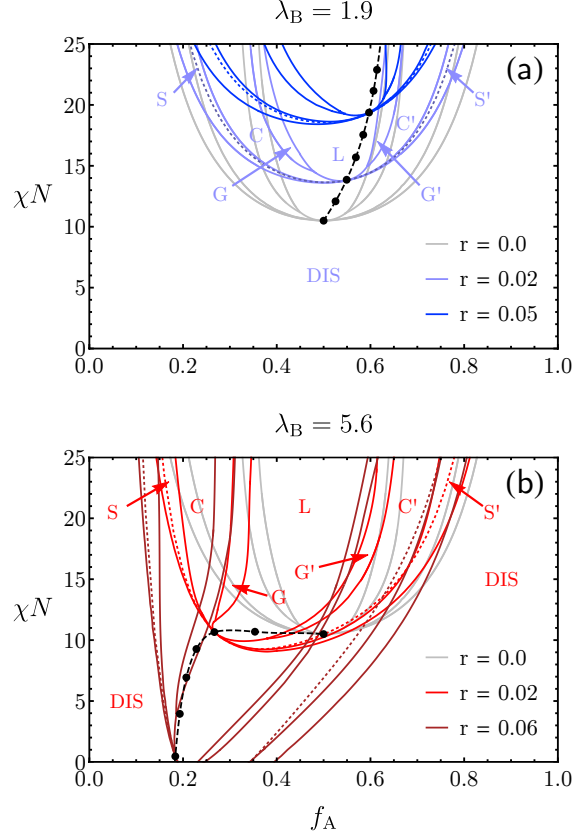
11

Figure 1: SCFT phase diagrams for salt-doped diblock copolymers according to the 'free-ion' model, showing the disordered phase (DIS), as well as lamellar (L), cylindrical (C), gyroidal (G), and BCC spherical (S) ordered phases. Ordered phases rich in component A are denoted with an apostrophe to distinguish then from B-rich phases, e.g., C and C'. Two distinct regimes of thermodynamic behavior are evident depending on the magnitude of the parameter $\lambda_B$. (a) For $\lambda_B < 3$, the translational entropy of ions dominates and ordered phases are destabilized. (b) For $\lambda_B > 4$, the ion solvation energy dominates and ordered phases are stabilized. Above, $f_A$ is the fraction of high-dielectric component in the diblock, $\chi N$ is the inter-block segregation strength, and $r$ is the dimensionless ion concentration, equivalent to the molar ratio of cations to the number of monomeric repeat units of the PEO-like block A. These diagrams were generated using the parameters $R_g = 2.9$ nm, $\varepsilon_A = \varepsilon_{PEO} = 8.0$, $\varepsilon_B = \varepsilon_{PS} = 2.4$, $a_+ = 0.1$ nm, and $a_- = 0.36$ nm. Solid lines denote phase boundaries computed from SCFT, and dotted lines denote spinodal curves calculated using weak segregation theory (WST). Dashed lines connect critical points from WST.

and cannot be rationalized using an $r$-dependent effective $\chi$ parameter. This is a direct consequence of the coupling of ionic solvation energy to the *inverse* of dielectric permittivity. These shifts can be rationalized by examining the density profiles of ordered phases in the entropic and solvation regimes, provided in Fig. 2. These density profiles illuminate the principal difference between the two regimes. In the entropic regime, ion translational entropy dominates and ions cannot be completely localized to the high dielectric phase. Because the ions cannot be readily confined, the system favors demixing, as the resulting average dielectric permittivity lowers the overall solvation energy. However, in the solvation regime, the ion solvation energy dominates and ions readily localize into the high dielectric phase. In this regime, the system can reduce its solvation energy by forming ordered phases with locally high dielectric constants, as ions are able to remain confined within these high dielectric microphases.

We emphasize that the behavior observed in the entropic regime is distinct from the neutral solvent dilution effect. In the latter, which can be realized in our model by setting $\lambda_B = 0$, the 'neutral solvent' ions localize near the lamellar interface, in order to dilute the number of contacts between incompatible monomers.[48] This is clearly demonstrated by Fig. 2a. Such screening tends to destabilize ordered phases, and results in a vertical and symmetric shift in the phase diagram, in contrast to more dramatic, asymmetric shifts evident in the ionic systems seen in Fig. 1.

Our previous screening of experimental parameters suggests that nearly all experimental systems fall into the solvation regime. In particular, SEO/LiTFSI, which will be the focus of the rest of this work, should have $\lambda_B \approx 10\,$–$\,100$ depending on the value of the ionic solvation radii, a point which will be further discussed below. This places SEO/LiTFSI squarely within the solvation regime, which is consistent with the experimental observation that lithium ions segregate almost exclusively into PEO-rich domains.[34]

Before applying our model to analyze SEO systems, it is instructive to first identify invariant parametric groups. The thermodynamic behavior of neat diblocks is governed by the
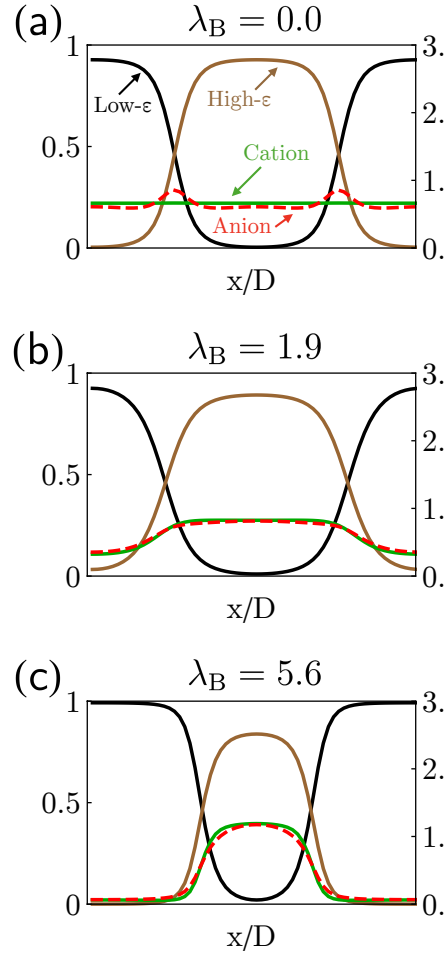
Figure 2: Lamellar-phase density profiles from SCFT. Polymer volume fraction is plotted on the left vertical axis. Ion concentrations are plotted on the right vertical axis, in units of mol/L. All plots were generated with $\chi N = 20$ and $r = 0.05$. (a) Diblock copolymer with 'neutral solvent' ions, $f_A = 0.5$. Ions segregate into the polymer interface. (b) Entropic regime, $f_A = 0.55$. Ions are delocalized across the ordered microphase. (c) Solvation regime, $f_A = 0.35$. Ions are concentrated in the microdomain with higher dielectric permittivity. All other parameters are the same as those in Fig. 1.

composition $f$ and the product $\chi N$, and that of neutral-solvent doped copolymers is governed by $f$ and $(1 - \phi_{\text{solvent}})\chi N$ in the weak segregation regime. By contrast, ion-containing diblock copolymers require more dimensionless groups. Composition is determined by the block fraction $f$, as well as the molar ion concentration $r$. Electrostatic interactions introduce two additional lengthscales; the Born solvation energy scales with ionic radius, $a$, and the pairwise Coulomb potential energy scales with the polymer lengthscale $R_{\text{g}}$. Thus, the three terms in the interaction free energy, Eq. (3), scale with $\chi$, $r l_{\text{B}}/a$, and $r^2 l_{\text{B}}/D$ respectively, where $l_{\text{B}} = \text{e}^2/(4\pi\varepsilon_{\text{r}} k_{\text{B}} T)$ is the Bjerrum length, and $D$ is the equilibrium domain spacing which scales with $R_{\text{g}}$. Noticing further that the ideal chain contribution to the free energy, found in Eq. (2), scales inversely with the molecular weight $N$, we conclude that in general, there is no simple choice of invariant groups to describe this system. Because both the Bjerrum length $l_{\text{B}}$ and composition $f$ are determined by the choice of polymer, we are left with three independent parameters $r$, $\chi$, and $N$ which jointly determine the phase behavior of ion-doped copolymers. In the following sections, we will address the impacts of each of these parameters, with a focus on the effects of the degree of salt doping $r$ and the molecular weight $N$.

## Parameterization of experimental data

Comparisons between theory and experiment are heavily dependent on the methodology used to map experimental measurements to theoretical parameters. The majority of parameters used in our ionic polymer self-consistent field theory (iPSCF) calculations are tabulated in Table 2 and are taken from compiled data for SEO/LiTFSI.[14]

We begin our analysis by accounting for the incompatibility between the PS and PEO blocks. Our theory makes use of the Flory-Huggins parameter $\chi$, which describes interactions in SEO copolymers without added salts. Experimentally, it has been observed that $\chi$ is a function of both the chain length, $N$, and temperature, $T$. We use the experimental fit

reported in Teran et al.[13]

$$\chi(N, T) = A(T) + \frac{B(T)}{N} = \frac{1}{T}\left(10.2\,\text{K} + \frac{1850\,\text{K}}{N}\right) \tag{10}$$

Eq. (10) is then used as an input to the iPSCF calculation to impose an intrinsic incompatibility between the PS and PEO blocks that is *unchanged* by the addition of ions. We emphasize that this is distinct from the effective $\chi$ employed in salt-doped systems.[13,14]

The reference volume $v_0 = 0.1\,\text{nm}^3$, which is needed to scale monomeric properties, was chosen to match the convention used to analyze experimental data.[8,13,14] The statistical segment lengths $b_\text{i}$ are calculated from the packing lengths $p_\text{i}$ by applying the relation[49] $p_\text{i} = v_0/b_\text{i}^2$, where $i$ is PS or PEO. The dielectric permittivities of PS and PEO are set to the experimentally measured values of $\varepsilon_\text{PEO} = 8.0$ and $\varepsilon_\text{PS} = 2.4$.[50,51]

For simplicity, we assume ideal mixing, such that the molecular volumes of ions and polymer are constant. The ionic volumes of Li$^+$ and TFSI$^-$ are chosen to match experimental measurements of the density of PEO homopolymer melts with varying concentrations of added LiTFSI salts.[35,52] Assuming that the ions can be approximated as hard spheres, the radii of Li$^+$ and TFSI$^-$ are 1.0 and 3.8 Å, respectively, which correspond to ionic volumes of $0.0042\,\text{nm}^3$ and $0.230\,\text{nm}^3$ for Li$^+$ and TFSI$^-$, respectively.

Table 2: Parameters used in iPSCF calculation.

| Parameter | Symbol | Value | Selection method |
|---|---|---|---|
| temperature | $T$ | 373 K | match[8] |
| Flory-Huggins, $\chi$ | $\chi$ | $\chi(N,T)$ | Eq. (10)[13] |
| reference volume | $v_0$ | $0.1\,\text{nm}^3$ | match[8] |
| statistical segment length (PEO) | $b_\text{PEO}$ | 0.73 nm | packing length[49] |
| statistical segment length (PS) | $b_\text{PS}$ | 0.50 nm | packing length[49] |
| permittivity (PEO) | $\varepsilon_\text{PEO}$ | 8.0 | measured[50] |
| permittivity (PS) | $\varepsilon_\text{PS}$ | 2.4 | measured[51] |
| ionic volume (Li) | $v_\text{Li}$ | $0.0042\,\text{nm}^3$ | ~~hard sphere volume~~ ideal mixing[52] |
| ionic volume (TFSI) | $v_\text{TFSI}$ | $0.230\,\text{nm}^3$ | ~~hard sphere volume~~ ideal mixing[52] |
| solvation radius (Li) | $a_\text{Li}$ | 1.43 nm | **fit to data** |
| solvation radius (TFSI) | $a_\text{TFSI}$ | 5.43 nm | **fit to data** |
| solvation parameter | $\lambda_\text{B}$ | 5.8 | Eq. (9) |

Out of the parameters in Table 2, the ion solvation radii $a_i$'s are the only parameters that cannot be directly measured. Although $a_{Li}$ and $a_{TFSI}$ define lengthscales, the effect of these parameters is to set the magnitude of the ion solvation free energy. Thus, this 'solvation radius' may not be directly related to the physical radii of each ion. For example, the solvation radius of an ion in water at least partially accounts for the size of its solvation shell.[41] Given the difficulty of measuring or cleanly defining this parameter, we treat it as adjustable, and fit it to match iPSCF phase diagrams to the experimental data at the order-disorder transition. This fitting methodology effectively absorbs complex ion solvation effects into the Born solvation radius, potentially capturing higher-order effects such as strong ionic correlations. To eliminate uncertainty in fitting, the ratio of solvation radii was kept constant at $a_{TFSI}/a_{Li} = 3.8$, which reproduces the ratio of hard-sphere volumes assigned to $v_{Li}$ and $v_{TFSI}$ in Table 2. Such an approach is justified because the magnitude of ionic solvation in iPSCF is jointly determined by the sum $(1/a_{Li}+1/a_{TFSI})$ in Eq. (9), which reflects the physical observation that Coulombic interactions prevent large-scale charge separation, i.e. cations and anions remain in close proximity and jointly determine the magnitude of the solvation energy.

Further details of the solvation fitting methodology can be found in the Supporting Information, and are schematically illustrated in Fig. S1. The best global fit was found at $\lambda_B = 5.8$ by fitting all of the copolymers in Table 1 simultaneously. In the rest of this manuscript, we use $\lambda_B = 5.8$ in all iPSCF calculations, as this represents the best fit through the entire dataset and places SEO/LiTFSI squarely in the solvation regime. This corresponds to solvation radii of $a_{Li} = 1.43\,\text{nm}$ and $a_{TFSI} = 5.43\,\text{nm}$. These large fitted solvation radii indicate that ionic solvation in polymeric media is much weaker than that predicted by the Born model, and highlights the need for more detailed models of ionic solvation in polymers.

# $f$-$r$ phase diagrams

One comparison between iPSCF prediction and experimental measurements is displayed in Fig. 3, for SEO/LiTFSI at two chain lengths $N = 45$ and 200, and at a fixed temperature 373 K. Presenting the comparison in $f$-$r$ plane bypasses the need of relating salt concentration to $\chi$ parameter. Experimental morphology data[8,13] for polymers with similar molecular weights are overlaid on the iPSCF phase diagrams as symbols: diamonds represent disordered phases (DIS), squares represent lamellar phases (L), triangles represent cylindrical and inverted cylindrical phases (C/C'), crosses represent gyroid and inverted gyroid phases (G/G'), and circles represent spherical and inverted spherical phases (S/S').

A surprising, qualitative agreement is revealed by the comparison. In the low molecular weight ($N = 45$) phase diagram, Fig. 3a, iPSCF captures both the order-disorder transition and the relative locations of many of the ordered phases. In particular, the order-disorder transition in an $f_{\mathrm{EO}}$-lean copolymer ($N = 42$, $f_{\mathrm{EO}} = 0.3$) occurs at a lower value of $r$ than compared to an $f_{\mathrm{EO}}$-rich copolymer ($N = 46$, $f_{\mathrm{EO}} = 0.54$), in agreement with experimental observations. However, the experimentally determined lamellar and cylindrical phases are shifted toward low $f_{\mathrm{EO}}$ relative to the iPSCF calculations, suggesting that the skewing of experimental data is more severe than predicted by iPSCF. The theory also predicts that, for a SEO copolymer with $f_{\mathrm{EO}}$ near 0.5, the lamellar phase should give way to the gyroid phase with increasing salt concentration $r$—note the curvature of the L/G' boundary on the $f_{\mathrm{EO}}$-rich side of the phase diagram in Fig. 3a. This order-to-order transition is observed experimentally, but at lower EO fraction, $f_{\mathrm{EO}} = 0.44$.

The high molecular weight ($N = 200$) phase diagram (Fig. 3b) is even more skewed than the low molecular weight phase diagram. Some support for this is contained in the experimental data. The salt concentration at which the order-to-disorder transition is obtained experimentally for the SEO copolymer with $f_{\mathrm{EO}} = 0.20$ is $r = 0.038$ (the average of the last disordered sample and the sample that is a cylindrical morphology) while that of the $f_{\mathrm{EO}} = 0.29$ sample occurs at $r = 0.008$. Both samples are close to the window where iPSCF
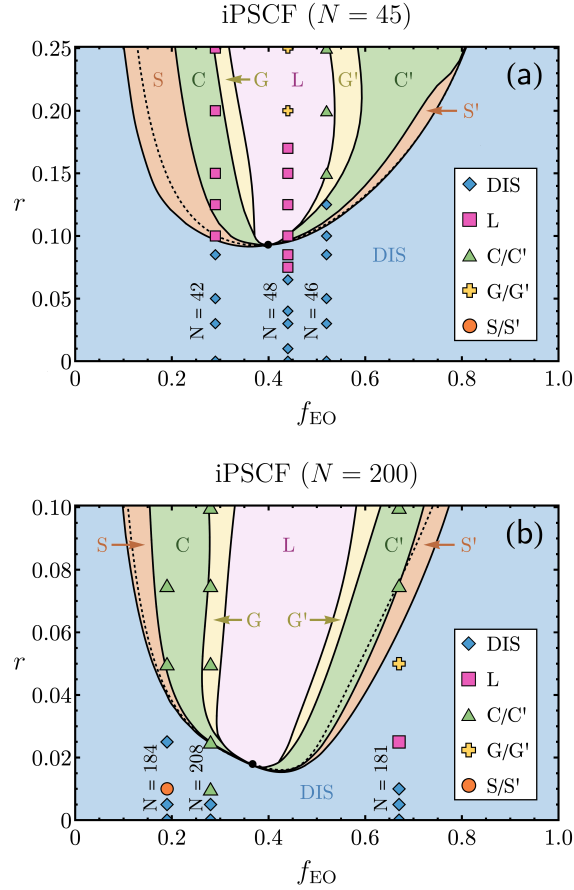
Figure 3: Comparison of phase behavior calculated by iPSCF with experimental data plotted in the $f$-$r$ plane at $373\,\mathrm{K}$. Stable morphologies predicted by iPSCF are indicated with a colored, shaded background. The theoretically determined limit of stability and critical point are labeled with a dashed black line and solid black point, respectively. Experimentally determined morphologies are labeled as symbols with the same coloring scheme. Both phase diagrams, computed at (a) $N = 45$ and (b) $N = 200$, otherwise use the same parameters (Table 2).

predicts a phase transition from disorder to cylindrical morphologies. Despite this agreement, iPSCF does not capture all observed behaviors. The $f_{\mathrm{EO}} = 0.68$ sample in Fig. 3b exhibits a series of phase transitions with increasing salt concentration, from disordered-to-lamellar-to-gyroidal-to-cylindrical phases. The experimental phase diagram of the $f_{\mathrm{EO}} = 0.29$ sample also contains a system where two coexisting spherical phases were obtained.[8] Neither of these phenomena are present in the iPSCF phase diagram. Nevertheless, the agreement between theory and experiment seen in Fig. 3 is noteworthy given the use of only a single fitting parameter, $\lambda_{\mathrm{B}}$.

# $N$-$r$ **Phase Diagrams**

Fully capturing the phase behavior of ion-containing copolymers requires three parameters: the block fraction $f_{\mathrm{EO}}$, salt concentration $r$, and chain length $N$. To illustrate this point, Fig. 4 shows a three-dimensional phase diagram for SEO/LiTFSI as a function of $f_{\mathrm{EO}}$, $r$, and $N$. Included in Fig. 4 are the two phase diagrams in the $f$-$r$ plane originally presented in Fig. 3. Planes in the $N$-$r$ space are shown at $f_{\mathrm{EO}} = 0.3$, $0.5$ and $0.7$, and the phase boundaries calculated by iPSCF are drawn to connect the low (black) and high (red) molecular weight phase diagrams at these compositions. It is obvious that the variation of phase behavior does not scale linearly with $N$ or $r$. This is largely due to asymmetric shifts in the phase diagram with respect to $f_{\mathrm{EO}}$, seen previously in Fig. 3, which are a direct consequence of the nonlinear form of the ionic solvation energy.

Figure 5 shows the comparison between iPSCF calculations and experimental data[8,14] for the $f_{\mathrm{EO}}$-lean SEO copolymers in the $N$-$r$ plane. The format of the phase diagrams mirrors that of Fig. 3: The phase boundaries calculated by theory are given by solid lines and the experimental data are superimposed on the corresponding $N$-$r$ phase diagrams. The colors and symbols used for each morphology match the colors used in Fig. 3. In Fig. 5a, we show the phase boundaries calculated from iPSCF at $f_{\mathrm{EO}} = 0.25$. The disordered, spherical,
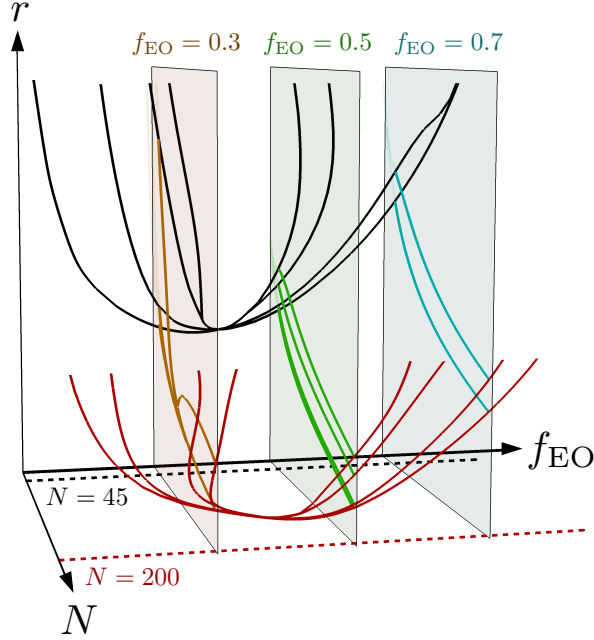
Figure 4: The phase diagrams from Figs. 3, 5 and 6 (below), represented within a three-dimensional phase space defined by $f_{EO}$, the copolymer composition, $N$, the chain molecular weight, and $r$, the ion concentration. Two-dimensional phase diagrams (Figs. 3, 5, and 6) correspond to isoplanes with fixed $N$ or fixed $f_{EO}$. These are shown in the 3D phase space to highlight the difficulty of collapsing phase diagrams onto a universal 2D representation.

cylindrical, and gyroid morphologies appear as expected.

Fig. 5b shows the phase boundaries calculated from iPSCF at $f_{EO} = 0.3$. In this case, the phase diagram is dominated by the gyroid phase. This is not usually seen in conventional phase diagrams shown in the $\chi N$ plane where the gryoid phase typically occupies a small area between the lamellar and cylindrical phases. The presence of the wide gyroid window originates from the construction of the isoplanes with constant $f_{EO}$, which are 'slices' nearly parallel to the phase boundaries; in the case of $f_{EO} = 0.3$ the slice extends through the gyroid phase. Note that a small change in $f_{EO}$ from 0.25 to 0.30 results in a drastic change in the phase behavior, as is evident in Figs. 5a and 5b. Therefore, mapping experimental data onto predictions in the $N$-$r$ plane is susceptible to small errors or inconsistencies in the parameterization of $f_{EO}$.

One potential source of inconsistency in $f_{EO}$ is non-ideal mixing of SEO with LiTFSI salts.[52] In our model, the volume of ions is assumed to be constant. However, changes in

the partial molar volume of EO monomers with the addition of salt are expected to produce small changes in the parameterized value of $f_{\mathrm{EO}}$. Proper accounting of this non-ideal mixing is an interesting future direction, but is beyond the scope of this work.
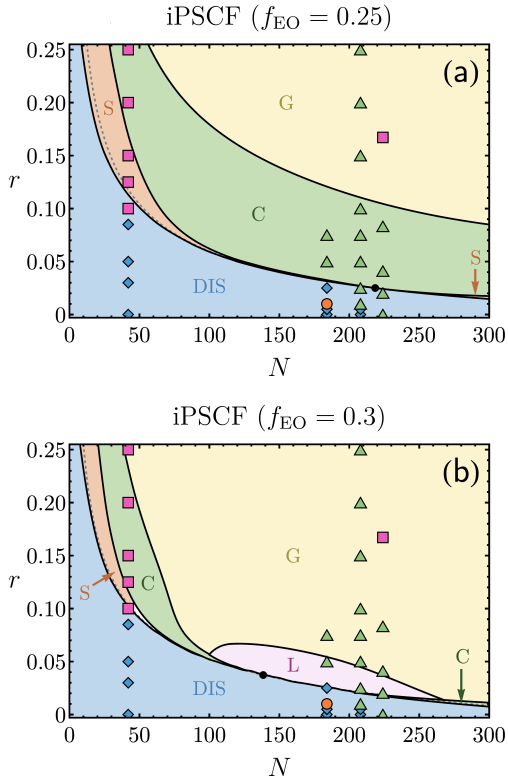


Figure 5: iPSCF phase diagrams (solid lines and shaded regions) plotted against the chain length, $N$, and the ion concentration, $r$, for (a) $f_{\mathrm{EO}} = 0.25$ and (b) $f_{\mathrm{EO}} = 0.30$, using the parameters in Table 2. Both figures show the experimental data (discrete symbols) for $0.20 \leq f_{\mathrm{EO}} \leq 0.30$ found in Table 1. The colors and symbols match those used in Fig. 3. The spinodal curve and critical point, obtained from RPA, are overlaid as a dashed black line and solid point, respectively. Note that iPSCF phase boundaries (solid lines) are extrapolated for $N > 200$.

The experimental data in both phase diagrams in Fig. 5 are identical and represent the range $0.2 \leq f_{\mathrm{EO}} \leq 0.3$ from Table 1. The experimental dataset at $N = 184$ has a composition of $f_{\mathrm{EO}} = 0.20$. The other experimental data sets correspond to $0.29 \leq f_{\mathrm{EO}} \leq 0.30$. For $N = 42$ and 184, there is good agreement between experiment and theory for the locations of the order-disorder boundaries in both Figs. 5a and 5b. There is however, a mismatch of sequence and location of the ordered phases. For example, theory predicts the existence

of stable lamellar phases at low salt concentrations for $f_{\rm EO} = 0.3$, but experiments show a lamellar phase appearing at higher salt concentrations. We attribute such discrepancies to the extreme sensitivity of phase diagrams in the $N$-$r$ plane to the parameterization of $f_{\rm EO}$. The $N = 184$ dataset agrees remarkably well with the theoretical phase diagram at $f_{\rm EO} = 0.25$. As seen in Fig. 5a, the experimentally determined disorder-to-cylinder boundary is in quantitative agreement with theory.

Figure 6 shows phase diagrams in the $N$-$r$ plane for SEO/LiTFSI systems with higher $f_{\rm EO}$ values. In Fig. 6a, the theoretical predictions at $f_{\rm EO} = 0.5$ are compared with experimental data obtained at $f_{\rm EO} = 0.44$ and 0.52. The data obtained at $N = 42$ corresponds to $f_{\rm EO} = 0.44$. All other data in Fig. 6a correspond to $f_{\rm EO} = 0.52$. The theoretical phase diagram for $f_{\rm EO} = 0.5$ is unsurprisingly dominated by the lamellar phase, which agrees well with experimental data. At $N = 42$ and $f_{\rm EO} = 0.44$, we observe a transition from disorder to cylinders experimentally. The theory predicts this transition from disorder to cylinders, followed by a cylinders to lamellae transition which is not observed experimentally. For $N > 30$, the theory predicts narrow windows over which non-lamellar phases are stable near the order-disorder boundary. The experimental data obtained at $N > 42$ show direct transitions from disorder to lamellae. At $N = 94$, gyroidal and cylindrical phases are obtained at high salt concentrations, whereas theory predicts lamellae. These discrepancies are likely due to theoretical sensitivity to the parameterization of $f_{\rm EO}$.[52]

In Fig. 6b, the theoretical predictions at $f_{\rm EO} = 0.7$ are compared with experimental data obtained at $f_{\rm EO} = 0.68$, $N = 181$ and $f_{\rm EO} = 0.72$, $N = 269$. The theoretical phase diagram is dominated by the cylindrical phase (C')—the location of which is in remarkable agreement with experimental data. In contrast, the experimental data exhibits disordered-to-lamellar-to-gyroid-to-cylinder transitions; the lamellar and gyroidal phases are observed over a narrow range of salt concentrations. The theoretically predicted transition from disorder to cylinders at a given value of $N$ is interrupted by a narrow window of spheres, which is not seen in the experimental data. This discrepancy cannot be rationalized by small shifts in $f_{\rm EO}$ alone,
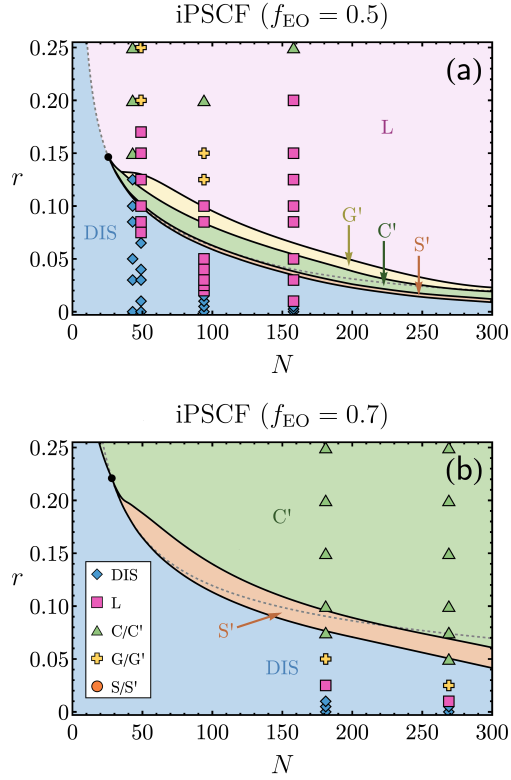
Figure 6: iPSCF phase diagrams (solid lines and shaded regions) plotted against the chain length, $N$, and the ion concentration, $r$, for (a) $f_{EO} = 0.50$ and (b) $f_{EO} = 0.70$. The format of Fig. 6 matches that of Fig. 5. The experimental data in (a) represent the range $0.44 \leq f_{EO} \leq 0.52$ and that in (b) represents the range $0.68 \leq f_{EO} \leq 0.72$ found in Table 1. Note that iPSCF phase boundaries (solid lines) are extrapolated for $N > 200$.

and may be worth probing in the future.

Both experimental data and the iPSCF results show that, the degree of salt doping $r$ at the ordering transition decreases with molecular weight $N$, while the corresponding salt-free ($r = 0.0$) systems do not order over the same range of molecular weights. Moreover, it is rather surprising that, with only one adjustable parameter in the solvation strength $\lambda_{\mathrm{B}}$, this dependence is captured by the iPSCF calculation within the range explored. Resolving the ordered phases in the high molecular weight regime requires ever increasing numerical precision. The boundaries for $200 < N < 300$ in both Figs. 5 and 6 are obtained by extrapolation. These extrapolations suggest that universal phase behavior is obtained in the high-$N$ limit. However, establishing phase behavior in this limit will require the development of ionic strong segregation theory (SST).[53]

The strong dependence of salt-induced ordering on molecular weight may be attributed to at least two factors. First, the product of the Flory-Huggins parameter for salt-free systems, Eq. (10), with molecular weight $\chi_0 N$ increases with $N$, which implies a stronger tendency of ordering in systems with higher molecular weights. As a result, a lower level of salt-doping is needed to induce the transition. Second, the ideal chain contribution to the free energy in Eq. (2), which favors the disordered phase, is smaller than all other free energy terms, specifically the solvation term, by a factor $1/N$. Therefore, with increasing molecular weight, less chain conformational entropy (per monomer) is penalized upon ordering and, again, a lower level of salt-doping is needed. This second point is consistent with the argument of a linear increment of $\chi_{\mathrm{eff}}$, but is more general in that the contribution of solvation goes beyond the correction to the quadratic term in the free energy, as shown in our preliminary weak segregation theory.[17]

In Fig. 6, the boundaries between ordered and disordered phases appear to converge towards a constant value in the large $N$ limit. In this strong-segregation regime, the interfacial region between PS-rich and PEO-rich domains sharpens and narrows, whereby the net charge or dipole density accumulates. Although we are unable to numerically calculate the phase

boundary in this regime, we expect that the ordering will occur at sufficiently high value of $N$, in accordance with the observation that neutral block copolymers with $\chi_0 > 0$ will order at sufficiently high molecular weights. At the same time, we hypothesize that the accumulated interfacial charge or dipole *opposes* ordering, which adds a free energy contribution that scales with $r^2$. Developing ionic strong segregation theory would help to elucidate the ordering behavior in this regime.

On the other hand, in the small $N$ limit, composition fluctuations, which are neglected in iPSCF, are expected to become important. Such fluctuations destabilize the ordered phase, and are expected to compete with the solvation-induced stabilization shown in Fig. 1. Although the competition between fluctuation and solvation has yet to be analyzed, qualitatively, we expect the solvation parameter $\lambda_B$ to depend on the treatment of fluctuations. This parameter was fit to the experimentally ordering transition by treating ion solvation radius as adjustable. If fluctuation effects play a significant effect in destabilizing ordered phases, then the fit solvation radius will underestimate the actual strength of ionic solvation. This may eliminate the need for the unusually large ($\approx 1\,\text{nm}$) solvation radii in Table 2.

## Conclusions

We have presented a systematic comparison between our recently developed ionic polymer self-consistent theory (iPSCF)[17] and the compiled experimental data[14] for SEO diblock copolymers doped with lithium salts. This theory accounts for ion solvation free energy, ion translational entropy, and Coulombic ion-ion interactions. We adopt a minimal modeling approach, using the simple Born solvation model with linear dielectric mixing to account for solvation in block copolymers. Unlike previous theories, we choose not to explicitly incorporate ion binding[10–12] or ionic structure[16,19–23] into the model, and instead absorb these effects into a fitted Born solvation radius. This approach allows us to focus on the extent to which ionic solvation ~~explains~~ can explain the phase behavior of ion-containing

block copolymers.

Such comparisons are more challenging than analogous comparison for neat diblock copolymers and those diluted with neutral solvents. The phase behavior of neat diblock copolymers is specified by $\chi N$ and $f$. That of neutral solvent-diluted systems, upon the use of the dilution approximation, is described by the product $(1-\phi_\mathrm{s})\chi N$ and the composition $f$, where $\phi_\mathrm{s}$ is the volume fraction of neutral solvent. For ion-doped systems, the parameter space is greatly expanded. Even if the block copolymer composition, dielectric permittivity, and solvation radii are all fixed, three parameters are still needed: inter-block incompatibility $\chi$, molecular weight $N$, and degree of ion-doping $r$ (Fig. 4). These three design parameters are readily tuned in experiments, and are the focus of this work.

This treatment leaves us with one free parameter, the strength of solvation free energy, which is set by the solvation radii of cations and anions (the two radii jointly determine the solvation free energy strength through Eq. (9)). We find that, by adjusting this single solvation parameter, the iPSCF theory captures qualitatively the morphological behaviors of two molecular weights over a wide range of copolymer compositions and salt concentrations (Fig. 3). Our best fit to experimental data places the solvation parameter at $\lambda_\mathrm{B} = 5.8$, which places SEO/LiTFSI squarely in the aforementioned solvation-driven regime. Given the simplicity of the model, this clearly suggests that ion solvation is the dominating interaction for salt-doped SEO.

A popular empirical approach[6,29,54] to account for the effects of salt-doping is to introduce an effective interaction parameter $\chi_\mathrm{eff}$ that increases linearly with salt concentration and is independent of the block copolymer composition, $f$. We assert that that the effect of added salt on the thermodynamics of block copolymers is asymmetric with respect to composition; a simple linear shift in $\chi_\mathrm{eff}$ cannot account for the complexities seen in both the experiments and theory presented here. This asymmetry can be accounted for empirically by postulating a composition-dependent parameter $m$, but the physical origin of this dependence remains unclear.[55] In contrast, the iPSCF model predicts asymmetric behavior with composition-

independent inputs listed in Table 2—a more detailed analysis can be found in the Supporting Information. We emphasize that our simple model produces asymmetric phase behavior with respect to copolymer composition using only the Born solvation model, without accounting for complex interactions such as ionic correlations or Li-EO complexation. The lack of perfect agreement between iPSCF predictions and theory suggests this work is a stepping stone towards the development of a robust understanding of thermodynamic interaction in block copolymer electrolytes.

We close by drawing attention to the limitations of our treatment of the ion solvation free energy, which parameterizes the free energy cost of dissolving an ion in a homogeneous dielectric medium with an adjustable Born solvation radius. The primary advantage of this approach is simplicity. This approach, however, does not explicitly incorporate effects such as ion clustering, which are likely to be important in all polymer electrolytes. These effects are partially absorbed into our fitting of the Born solvation radii, and may help to rationalize the weakening of Born solvation as resulting from the use of large solvation radii. Recent experiments and simulations show that ion transport in PEO/LiTFSI mixtures can, in concentrated regimes (e.g. $r \sim 0.1$), be dominated by negatively charged clusters.[35–38] In other words, lithium ions are "solvated" by multiple negatively charge bulky anions rather than just ether oxygens. As a result, the solvation free energy of an ion depends not only on the properties of the solvating medium, but the presence and concentration of other ions. Such effects may help rationalize the need of a solvation radius of order $1\,\mathrm{nm}$. These ionic structures, as well as the effects of ion binding, require treatment of interactions at the molecular length scale. At these small length scales, the continuum dielectric permittivities used in our model also require correction. Though the permittivity may be self-consistently embedded by employing field theories with explicit polarization,[56,57] such models also require additional adjustable parameters, i.e. dipole moments and/or polarizabilites which must be validated against simulations or detailed experimental measurements. Using atomistic simulations, which do not require *ad hoc* adjustable parameters, to compute the solvation

free energy of various lithium salts dissolved in oligo-ethylene oxide would help to resolve ~~this,~~ these molecular scale issues, and provide a means for incorporating more sophisticated descriptions of ion-ion and ion-solvent interactions into the iPSCF theory.

# Acknowledgement

# Supporting Information Available

Additional details of solvation parameter fitting methodology, as well as supplementary analysis of the effective $\chi$ parameter.

# References

(1) Matsen, M. W.; Bates, F. S. Unifying weak- and strong-segregation block copolymer theories. *Macromolecules* **1996**, *29*, 1091–1098, DOI: `10.1021/ma951138i`.

(2) Fredrickson, G. *The Equilibrium Theory of Inhomogeneous Polymers*; Oxford Unversity Press, 2013.

(3) Khandpur, A. K.; Foerster, S.; Bates, F. S.; Hamley, I. W.; Ryan, A. J.; Bras, W.; Almdal, K.; Mortensen, K. Polyisoprene-polystyrene diblock copolymer phase dia-

gram near the order-disorder transition. *Macromolecules* **1995**, *28*, 8796–8806, DOI: `10.1021/ma00130a012`.

(4) Qin, J.; Bates, F. S.; Morse, D. C. Phase behavior of nonfrustrated ABC triblock copolymers: weak and intermediate segregation. *Macromolecules* **2010**, *43*, 5128–5136, DOI: `10.1021/ma100400q`.

(5) Lauter, U.; Meyer, W. H.; Wegner, G. Molecular composites from rigid-rod poly(p-phenylene)s with oligo(oxyethylene) side chains as novel polymer electrolytes. *Macromolecules* **1997**, *30*, 2092–20101, DOI: `10.1021/ma961098y`.

(6) Gunkel, I.; Thurn-Albrecht, T. Thermodynamic and structural changes in ion-containing symmetric diblock copolymers: a small-angle X-Ray scattering study. *Macromolecules* **2012**, *45*, 283–291, DOI: `10.1021/ma201334h`.

(7) Epps, T. H.; Bailey, T. S.; Hoai, D. P.; Bates, F. S. Phase behavior of lithium perchlorate-doped poly(styrene-b-isoprene-b-ethylene oxide) triblock copolymers. *Chem. Mater.* **2002**, *14*, 1706–1714, DOI: `10.1021/cm010971t`.

(8) Loo, W. S.; Jiang, X.; Maslyn, J. A.; Oh, H. J.; Zhu, C.; Downing, K. H.; Balsara, N. P. Reentrant phase behavior and coexistence in asymmetric block copolymer electrolytes. *Soft Matter* **2018**, *14*, 2789–2795, DOI: `10.1039/C8SM00175H`.

(9) Wang, Z.-G. Effects of ion solvation on the miscibility of binary polymer blends. *J. Phys. Chem. B* **2008**, *112*, 16205–16213, DOI: `10.1021/jp806897t`.

(10) Nakamura, I.; Wang, Z.-G. Salt-doped block copolymers: ion distribution, domain spacing and effective $\chi$ parameter. *Soft Matter* **2012**, *8*, 9356, DOI: `10.1039/c2sm25606a`.

(11) Nakamura, I.; Balsara, N. P.; Wang, Z.-G. First-order disordered-to-lamellar phase transition in lithium salt-doped block copolymers. *ACS Macro Lett.* **2013**, *2*, 478–481, DOI: `10.1021/mz4001404`.

(12) Nakamura, I.; Wang, Z.-G. Thermodynamics of salt-doped block copolymers. *ACS Macro Lett.* **2014**, *3*, 708, DOI: `10.2021/mz500301z`.

(13) Teran, A. A.; Balsara, N. P. Thermodynamics of block copolymers with and without salt. *Journal of Physical Chemistry B* **2014**, *118*, 4–17, DOI: `10.1021/jp408079z`.

(14) Loo, W. S.; Balsara, N. P. Organizing thermodynamic data obtained from multicomponent polymer electrolytes: salt-containing polymer blends and block copolymers. *Journal of Polymer Science Part B: Polymer Physics* **2019**, *57*, 1177–1187, DOI: `10.1002/polb.24800`.

(15) Sing, C.; Zwanikken, J. W.; Olvera de la Cruz, M. Interfacial behavior in polyelectrolyte blends: hybrid liquid-state integral equation and self-consistent field theory study. *Phys. Rev. Lett.* **2013**, *111*, 168303–1–168303–5, DOI: `10.1103/PhysRevLett.111.168303`.

(16) Sing, C.; Zwanikken, J. W.; Olvera de la Cruz, M. Ion correlation-induced phase separation in polyelectrolyte blends. *ACS Macro Lett.* **2013**, *2*, 1042–1046, DOI: `10.1021/mz400511r`.

(17) Hou, K.; Qin, J. Solvation and entropic regimes in ion-containing block copolymers. *Macromolecules* **2018**, *51*, 7463–7475, DOI: `10.1021/acs.macromol.8b01616`.

(18) McQuarrie, D. *Statistical Mechanics*; University Science Books, 2000.

(19) Zwanikken, J. W.; Jha, P. K.; Olvera de la Cruz, M. A practical integral equation for the structure and thermodynamics of hard sphere Coulomb fluids. *J. Chem. Phys.* **2011**, *135*, 064106, DOI: `10.1063/1.3624809`.

(20) Sing, C.; Zwanikken, J. W.; Olvera de la Cruz, M. Electrostatic control of block copolymer morphology. *Nature Materials* **2014**, *13*, 694–698, DOI: `10.1038/nmat4001`.

(21) Sing, C.; Zwanikken, J. W.; Olvera de la Cruz, M. Polyelectrolyte blends and nontrivial

behavior in effective Flory-Huggins parameters. *ACS Macro Lett.* **2014**, *3*, 698–702, DOI: `10.1021/mz500202n`.

(22) Pryamitsyn, V. A.; Kwong, H.-K.; Zwanikken, J. W.; Olvera de la Cruz, M. Anomalous phase behavior of ionic polymer blends and ionic copolymers. *Macromolecules* **2017**, *50*, 5194–5207, DOI: `10.1021/acs.macromol.7b00523`.

(23) Brown, J. R.; Seo, Y.; Hall, L. M. Ion correlation effects in salt-doped block copolymers. *Phys. Rev. Lett.* **2018**, *120*, 127801–1–127801–7, DOI: `10.1103/PhysRevLett.120.127801`.

(24) Young, W.-S.; Brigandi, P. J.; Epps, T. H. Crystallization-induced lamellar-to-lamellar thermal transition in salt-containing block copolymer electrolytes. *Macromolecules* **2008**, *41*, 6276–6279, DOI: `10.1021/ma8014068`.

(25) Hallinan, D. T.; Balsara, N. P. Polymer electrolytes. *Annual Review of Materials Research* **2013**, *43*, 503–525, DOI: `10.1146/annurev-matsci-071312-121705`.

(26) Mogurampelly, S.; Ganesan, V. Influence of nanoparticle surface chemistry on ion transport in polymer nanocomposite electrolytes. *Solid State Ionics* **2016**, *286*, 57–65, DOI: `10.1016/j.ssi.2015.12.018`.

(27) Miller, T. F., III; Wang, Z.-G.; Coates, G. W.; Balsara, N. P. Designing polymer electrolytes for safe and high capacity rechargeable lithium batteries. *Acc. Chem. Res.* **2017**, *50*, 590–593, DOI: `10.1021/acs.accounts.6b00568`.

(28) Loo, W. S.; Galluzzo, M. D.; Li, X.; Maslyn, J. A.; Oh, H. J.; Mongcopa, K. I.; Zhu, C.; Wang, A. A.; Wang, X.; Garetz, B. A.; Balsara, N. P. Phase Behavior of Mixtures of Block Copolymers and a Lithium Salt. *Journal of Physical Chemistry B* **2018**, *122*, 8065–8074, DOI: `10.1021/acs.jpcb.8b04189`.

(29) Young, W.-S.; Epps, T. H. Salt doping in PEO-containing block copolymers: counterion and concentration effects. *Macromolecules* **2009**, *42*, 2672–2678, DOI: `10.1021/ma802799p`.

(30) Müller-Plathe, F.; van Gunsteren, W. F. Computer simulation of a polymer electrolyte: Lithium iodide in amorphous poly(ethylene oxide). *Journal of Chemical Physics* **1995**, *103*, 4745, DOI: `https://doi.org/10.1063/1.470611`.

(31) Mao, G.; Saboungi, M.-L.; Price, D. L.; Armand, M. B.; Howells, W. S. Structure of Liquid PEO-LiTFSI Electrolyte. *Physical Review Letters* **2000**, *84*, 5536, DOI: `10.1103/PhysRevLett.84.5536`.

(32) Eilmes, A.; Kubisiak, P. Polarizable Continuum Model Study on the Solvent Effect of Polymer Matrix in Poly(ethylene oxide)-Based Solid Electrolyte. *Journal of Physical Chemistry A* **2008**, *112*, 8849–8857, DOI: `https://doi.org/10.1021/jp8021166`.

(33) Borodin, O.; Smith, G. D. Mechanism of ion transport in amorphous poly(ethylene oxide)/LiTFSI from molecular dynamics simulations. *Macromolecules* **2006**, *39*, 1620–1629, DOI: `10.1021/ma052277v`.

(34) Gomez., E. D.; Panday, A.; Feng, E. H.; Chen, V.; Stone, G. M.; Minor, A. M.; Kisielowski, C.; Downing, K. H.; Borodin, O.; Smith, G. D.; Balsara, N. P. Effect of ion distribution on conductivity of block copolymer electrolytes. *Nano Lett.* **2009**, *9*, 1212–1216, DOI: `10.1021/nl900091n`.

(35) Pesko, D. M.; Timachova, K.; Bhattacharya, R.; Smith, M. C.; Villaluenga, I.; Newman, J.; Balsara, N. P. Negative Transference Numbers in Poly(ethylene oxide)-Based Electrolytes. *J. Electrochem. Soc.* **2017**, *164*, E3569–E3575, DOI: `10.1149/2.0581711jes`.

(36) Molinari, N.; Mailoa, J. P.; Kozinsky, B. Effect of salt concentration on ion clustering and transport in polymer solid electrolytes: a molecular dy-

namics study of PEO–LiTFSI. *Chem. Mater.* **2018**, *30*, 6298–6306, DOI: `10.1021/acs.chemmater.8b01955`.

(37) Wheatle, B. K.; Lynd, N. A.; Ganesan, V. Effect of polymer polarity on ion transport: a competition between ion aggregation and polymer segmental dynamics. *ACS Macro Lett.* **2018**, *7*, 1149–1154, DOI: `10.1021/acsmacrolett.8b00594`.

(38) Seo, Y.; Shen, K.-H.; Brown, J. R.; Hall, L. M. Role of Solvation on Diffusion of Ions in Diblock Copolymers: Understanding the Molecular Weight Effect through Modeling. *Journal of the American Chemical Society* **2019**, *141*, 18455–18466, DOI: `https://doi.org/10.1021/jacs.9b07227`.

(39) Nakamura, I. Ion Solvation in Polymer Blends and Block Copolymer Melts: Effects of Chain Length and Connectivity on the Reorganization of Dipoles. *J. Phys. Chem. B* **2014**, *118*, 5787–5796, DOI: `10.1021/jp502987a`.

(40) Liu, L.; Nakamura, I. Solvation energy of ions in polymers: effects of chain length and connectivity on saturated dipoles near ions. *J. Phys. Chem. B* **2017**, *121*, 3142, DOI: `10.1021/acs.jpcb.7b00671`.

(41) Israelachvili, J. N. *Intermolecular and Surface Forces*; Academic Press, 2011.

(42) Li, Z.; Dyk, A. K. V.; Fitzwater, S. J.; Fichthorn, K. A.; Milner, S. T. Atomistic molecular dynamics simulations of charged latex particle surfaces in aqueous solution. *Langmuir* **2016**, *32*, 428–441, DOI: `10.1021/acs.langmuir.5b0`.

(43) Sihvola, A. Mixing rules with complex dielectric coefficients. *Subsurface Sensing Technologies and Applications* **2000**, *1*, 393–415.

(44) Landau, L. D.; Lifshitz, E. M. *Statistical Physics: Part I*; Butterworth Heinemann, 1999.

(45) Liang, S.; Chen, Q.; Choi, U. H.; Bartels, J.; Bao, N.; Runt, J.; Colby, R. H. Plasticizing Li single-ion conductors with low volatility siloxane copolymers and oligomers containing ethylene oxide and cyclic carbonates. *Journal of Materials Chemistry A* **2015**, *3*, 21269, DOI: `10.1039/C5TA06042G`.

(46) Qin, J. Studies of Block Copolymer Melts by Field Theory and Molecular Simulation. Ph.D. thesis, University of Minnesota, 2009.

(47) Arora, A.; Qin, J.; Morse, D. C.; Delaney, K. T.; Fredrickson, G. H.; Bates, F. S.; Dorfman, K. D. Broadly accessible self consistent field theory for block polymer materials discovery. *Macromolecules* **2016**, *49*, 4675–4690, DOI: `10.1021/acs.macromol.6b00107`.

(48) Fredrickson, G. H.; Leibler, L. Theory of block copolymer solutions: nonselective good solvents. *Macromolecules* **1989**, *22*, 1238–1250, DOI: `10.1021/ma00193a040`.

(49) Fetters, L. J.; Lohse, D. J.; Milner, S. T. Packing length influence in linear polymer melts on the entanglement, critical, and reptation molecular weights. *Macromolecules* **1999**, *32*, 6847–6851, DOI: `10.1021/ma990620o`.

(50) Porter, C.; Boyd, R. A dielectric study of the effects of melting on molecular relaxation in poly(ethylene oxide) and polyoxymethylene. *Macromolecules* **1971**, *4*, 589–594.

(51) Yano, O.; Wada, Y. Dynamic mechanical and dielectric relaxations of polystyrene below the glass temperature. *Journal of Polymer Science A2* **1971**, *9*, 669–686.

(52) Loo, W. S.; Mongcopa, K. I.; Gribble, D. A.; Faraone, A. A.; Balsara, N. P. Investigating the Effect of Added Salt on the Chain Dimensions of Poly(ethylene oxide) through Small-Angle Neutron Scattering. *Macromolecules* **2019**, *52*, 8724–8732, DOI: `10.1021/acs.macromol.9b01509`.

(53) Semenov, A. N. Contribution to the theory of microphase layering in block-copolymer melts. *Sov. Phys. JETP* **1985**, *61*, 733–742.

(54) Wakanule, N. S.; Virgil, J. M.; Teran, A. A.; Wang, Z.-G.; Balsara, N. P. Thermodynamic properties of block copolymer electrolytes containing imidazolium and lithium salts. *Macromolecules* **2010**, *43*, 8282–8289, DOI: `10.1021/ma1013786`.

(55) Loo, W. S.; Sethi, G. K.; Teran, A. A.; Galluzzo, M. D.; Maslyn, J. A.; Oh, H. J.; Mongcopa, K. I.; Balsara, N. P. Composition Dependence of the Flory–Huggins Interaction Parameters of Block Copolymer Electrolytes and the Isotaksis Point. *Macromolecules* **2019**, *52*, 5590–5601, DOI: `10.1021/acs.macromol.9b00884`.

(56) Martin, J. M.; Li, W.; Delaney, K. T.; Fredrickson, G. H. Statistical field theory description of inhomogeneous polarizable soft matter. *J. Chem. Phys.* **2016**, *145*, 154104, DOI: `10.1063/1.4964680`.

(57) Grzetic, D. J.; Delaney, K. T.; Fredrickson, G. H. The effective $\chi$ parameter in polarizable polymeric systems: one-loop perturbation theory and field-theoretic simulations. *J. Chem. Phys.* **2018**, *148*, 204903, DOI: `10.1063/1.5025720`.

# Graphical TOC Entry